ORIGINAL PAPER

Effect of O-ring Deformation on Saturated Load Pressure of the Small Piezoelectric-Hydraulic Pump Brake System

Phuc Anh Nguyen[1] · Jai-Hyuk Hwang[1] · Jae-Sung Bae[1]

Abstract

This paper examines the effect of deformation of the O-ring on maximum pressure in the load side of the small piezoelectric-hydraulic pump brake system. In the previous study, the small piezoelectric-hydraulic pump braking system used for small- and medium-sized unmanned aerial vehicles was developed. To operate the brake system, load pressure must be formed. The magnitude of the load pressure is determined by the pressure in the chamber and the adapted check valve type. Therefore, a study of the parameters affecting the chamber pressure is necessary to improve the load side pressure. The volume change of the O-ring seal has a complicated effect on the maximum pressure in the chamber of the piezoelectric-hydraulic pump. Accordingly, this study analyzed the effect of the O-ring on chamber pressure, considering the changing volume of the O-ring seal with nonlinear property material. The deformation of the O-ring made of nitrile-butadiene rubber was investigated using the finite-element method. In addition, the optimal radius of the piston was determined to obtain the maximum chamber pressure. The obtained maximum pressure and optimal radius are verified by comparison with the pressurization experiment using the developed small piezoelectric-hydraulic pump brake system.

Keywords Piezoelectric-hydraulic pump · Load pressure · O-ring deformation · Smart material pump

1 Introduction

Due to the reliability, cost, safety of supply, and structural simplicity, aircrafts generally use hydraulic systems with power oil pressure as a mechanical power transmission medium. Aircraft brake systems using hydraulic systems commonly include complex components, such as a pressure accumulator, a hydraulic reservoir, solenoids valves, check valves, and electronic control devices, and so there is a limitation to applying the conventional hydraulic system to unmanned aircraft, which have stricter weight and space constraints. Consequently, the miniaturization of the brake system suitable to small- and medium-sized unmanned aerial vehicles demands a small-sized hydraulic pump which plays a crucial role in forming flow rate and load pressure. Recently, studies have been conducted on small-sized smart material pumps [1–3], and therefore, several types of

the smart material actuators such as ionic polymer–metal composites (IPMCs), shape memory alloy (SMA), and lead zirconate titanate (PZT) have been studied [4–6]. For the development of brake systems for small- to medium-sized unmanned aircrafts, the piezostack actuator is most applicable to build up a large load pressure with small displacement. Most piezoelectric micropumps are studied with piezoelectric membrane actuators (named piezomembrane pumps) for fluid delivery, such as the valve-less pumps [7–9], check valve pumps [10–12], and peristaltic pumps [13–15]. These piezomembrane pumps are characterized by their structure and small volume. Another kind of piezoelectric pumps is driven by piezostack actuators [16, 17] which are called piezoelectric-hydraulic pumps or piezostack pumps. Compared with the piezomembrane pumps, the piezoelectric-hydraulic pumps are able to achieve high backpressure and are applicable for high-power applications, especially for the piezoelectric-hydraulic linear actuators. Therefore, a previous study by this team developed and fabricated a small piezoelectric hydraulic pump with a PZT actuator used for UAV brake systems. Compared with a traditional pump, the piezoelectric-hydraulic pump has the advantages of a simple structure, low power

✉ Jai-Hyuk Hwang
jhhwang@kau.ac.kr

1 Department of Aerospace and Mechanical Engineering, Korea Aerospace University, 76 Hanggongdaehak-ro, Deogyang-gu, Goyang-si, Gyeonggi-do 10540, Republic of Korea

consumption, high reliability, and precise pressure control.

In the previous research, a small piezoelectric-hydraulic pump was designed to meet the brake system requirements of small- and medium-sized UAVs [18]. The exhaust flow rate, high pressure, fast response speed, and stable operation are one of these requirements. The pressurization performances of the pump were analyzed and verification experiments were carried out. Piezoelectric ceramic actuators can generate greater force than other smart material actuators and can operate at high speed. However, it is noted that the drawback coming from piezoelectric ceramic actuators is a very small mechanical displacement. Therefore, it is necessary to design a suitable check valve that can discharge the small flow rate of the piezoelectric-hydraulic pump in a single direction effectively. For the present study, a ball-thin plate spring-type check valve was designed to effectively transmit the small flow rate in the output direction. Moreover, it allows the valve to be opened easily whenever there is a pressure difference on the two sides of the check valve. In this case, the check valve has the ability to work well under the high-speed operation of the piezoceramic actuator. The check valve used in this study is a passive type one, so as to reduce the complexity of the system to satisfy the miniaturization and lightweight objectives of the research. The small piezoelectric-hydraulic pump is able to increase the driving frequency to obtain the required flow rate, even though the exhaust flow rate is very small [19–21].

Currently, there exists little research regarding piezoelectric-hydraulic pumps building up chamber pressure. Lindler [22] conducted an experiment to investigate the pressurization of hydraulic fluid. However, that research is based on the results of an experiment which does not show the factors affecting the results in formulas. This research presents attempts to formulate the equation for determining the saturated pressure at the load side and the pressurization

performance of the piezoelectric-hydraulic pump considering the effect of O-ring deformation is presented in this work. The pressure value at the load side is of interest to satisfy the condition of the brake system. The pressure at the load side is determined by the pressure in the chamber and the area ratio of the check valve used in the pump. The analytical equation for the chamber pressure which is helpful for calculating the load side pressure is derived based on the volumetric change due to O-ring deformation and liquid compressibility. The chamber pressure is affected by the displacement of the PZT actuator, the diameter of the piston, and the deformation of the O-ring seal which prevents leaks from occurring. For small pumps, the change in an O-ring's volume significantly influences the volume of the chamber, thus greatly affecting the compression process. The present work focused on accurately analyzing the effect of the O-ring's volumetric change due to the increasing pressure on the change in the chamber pressure. The Mooney–Rivlin model with a higher order term was adopted as an O-ring material. The effects of both the fractional compression of an O-ring and medium pressure on the change in chamber's volume were analyzed. For verification of analytical results, the piezoelectric-hydraulic pump was fabricated and tested. Furthermore, the optimal piston's dimension was determined to achieve the maximum chamber pressure.

2 Working Principle of the Piezoelectric-Hydraulic Pump Brake System

The piezoelectric-hydraulic pump brake system presented in this paper (Fig. 1) consists of a piezo stack actuator, two check valves, a piston, and a chamber space. When the PZT actuator is guided by fluctuating voltage, the piezoelectric-hydraulic pump can transfer mechanical energy into liquid flow. Table 1 illustrates the specifications of the PZT actuator used in

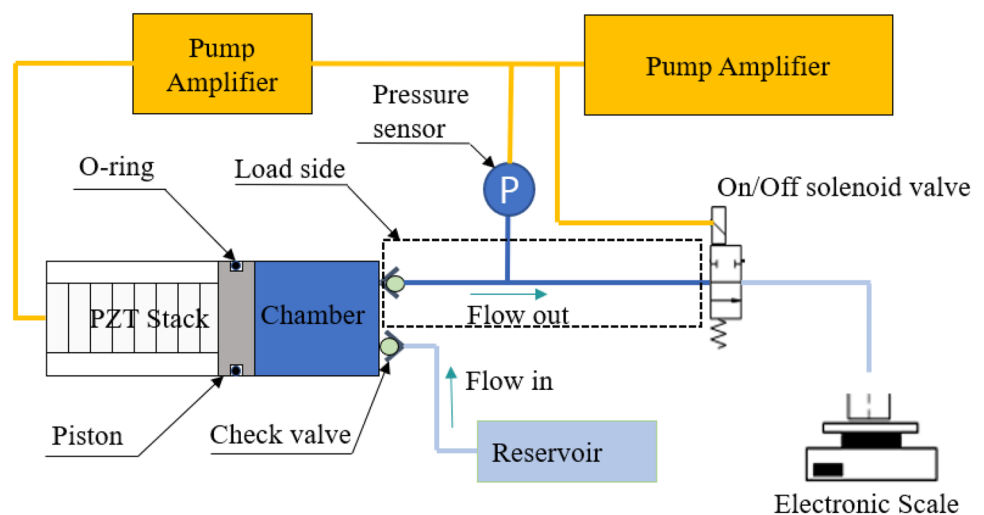Fig. 1 Schematic of the piezoelectric-hydraulic pump brake system

Table 1 Specifications of the PZT actuator

Piezo stack—Model P-225.40	
Operating voltage	0–1000 V
Closed-loop travel	60 μm
Unload resonant frequency	7 kHz
Push/pull force capacity	12,500/2000 N
Mass (with cable)	610 g

the piezoelectric-hydraulic pump. The chamber transmission part which connects the PZT actuator and liquid is a piston. When the PZT actuator is vibrating in extending-shrinking vibration mode, the compressed liquid in the chamber causes the check valve alternately open and close. Consequently, the liquid was transferred from the inlet to the outlet continuously.

In this study, the ball-type check valve, which allows the flow to discharge through when the pressure in the chamber is greater than the pressure in the load side, is designed to prevent liquid backflow. When the solenoid valve is opened, the flow rate test is performed. The amount of liquid is measured by the weight scale. By the analytical method, the flow rate is calculated by the formula:

$$Q = \Delta V \, f \, \eta, \tag{1}$$

where f denotes the driving frequency, ΔV refers to the volume deflection of the pump chamber (depends on the chamber dimension and the maximal displacement of PZT actuator under liquid pressure), and η is the check efficiency of the check valve. It should be noted that the check efficiency of check valves depends on operating frequency and valve type/size.

When the solenoid valve is closed, the pressurization test is conducted. The load pressure rises up with each upward stroke of the piston. Because the area ratio of the ball-type check valve has a value of 1, the load side pressure gradually increases until it is equal to the maximum pressure in the chamber. The chamber pressure can be calculated by the following:

$$\frac{\Delta V}{V_{\text{chamber}}} = -\frac{P_{\text{chamber}}}{B}, \tag{2}$$

where ΔV denotes the compressed liquid volume due to the piston movement which is proportional to the displacement, the radius of the piston; the O-ring's deformation which depends on the chamber pressure, the V_{chamber} refers to the chamber's volume, B is the bulk modulus of the liquid, and P_{chamber} denotes the chamber pressure. The relationship between the piston motion and the chamber pressure is shown in the formula:

$$m\ddot{x} + c\dot{x} + kx = F_{\text{a}} - P_{\text{chamber}} \, A_{\text{piston}}, \tag{3}$$

where m is the effective mass of the piston and actuator, c refers to the damping coefficient of the actuator, k denotes the stiffness of the actuator, x is the displacement of the piston, F_{a} and $P_{\text{chamber}} \times A_{\text{piston}}$ are the external force which is generated by the actuator and the chamber pressure, respectively. Equation (2) suggests that the chamber pressure is proportional with the compressed liquid volume being the product of the displacement and the area of the piston, so the chamber pressure rises up with the increase of the piston's radius and the displacement of the piston. On the other hand, Eq. (3) shows that the increase of the piston's radius could lead to a reduction of the pressure in the chamber and the displacement. Thus, there will be an optimal piston's radius for the piezoelectric-hydraulic pump brake system to achieve the maximum chamber pressure, i.e., the maximum pressure in the load side. In view of the above analysis, it is important to obtain the functional relationship between the piston's radius and the pressure in the chamber.

3 An Analytical Model for the Pressurization Process of the Piezoelectric-Hydraulic Pump Brake System

During the pressurization, the liquid flows through the inlet and fills in the chamber when the piston moves downward. The liquid starts being compressed in the chamber when the piston moves upward. If the pressure in the chamber is large enough to open the check valve, the liquid enters the load side through the outlet and the load pressure builds up. When the load pressure reaches the saturated value, it means that the check valve does not open and the oscillation of the piston due to the liquid in the chamber is compressed. The relationship between the fluctuation pressure and the amount of liquid discharging and entering through the inlet at each cycle is represented by Eq. (2).

According to the manufacturer's instructions, the dynamic operation of the piezoelectric actuators can be modeled as a mass–damper–spring system. This model includes the damping and effective masses of moving parts (piezo actuator and piston). The piezo effect can be modeled as an external force [16], proportional to the voltage, acting on the piston. The dynamic equation of the piston and actuator can be written as Eq. (3). In fact, the stiffness of the actuator (k) is much larger than the effective mass (m) and the damping (c), so the dynamic parts are neglectable. It means that Eq. (3) can lead to Eq. (4):

$$kx = F_{\text{a}} - P_{\text{chamber}} A_{\text{piston}}. \tag{4}$$

The upward movement of the piston compresses the liquid in the chamber and reduces the volume of the liquid in the chamber. The relationship between the reducing volume and

Fig. 2 The relationship between the chamber pressure and the bulk modulus
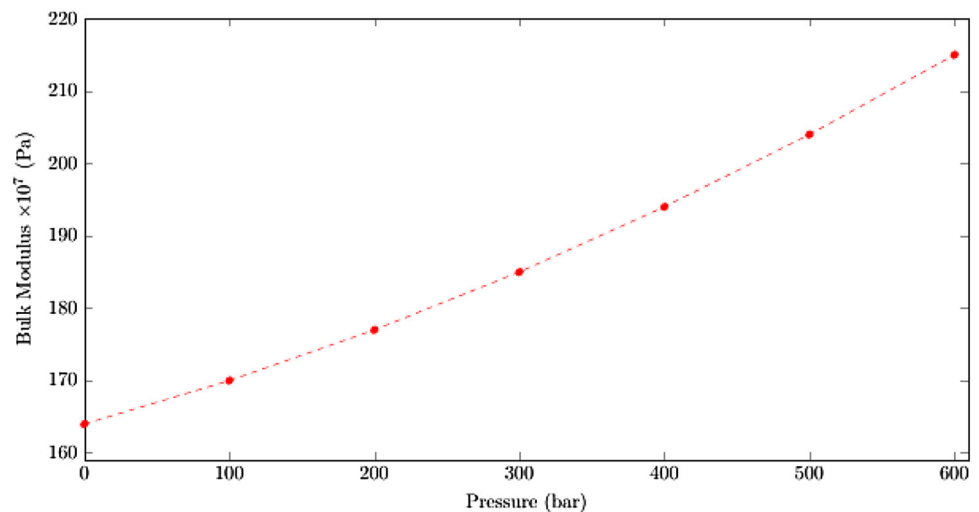
the pressure in the chamber is shown in Eq. (2). Because the piston has an O-ring to ensure that the liquid does not leak, the changed volume of the chamber includes the change of the compressed liquid and the change caused by O-ring deformation. The volumetric changes are expressed by the formula:

$$\Delta V = -x A_{\text{piston}} + V_{\text{o}}, \tag{5}$$

where A_{piston} denotes the area surface of the piston and V_{o} represents the changed volume caused by the O-ring deformation due to the chamber pressure. The compressibility of a liquid is characterized by bulk modulus parameter. The bulk modulus elasticity or volume modulus is a material property characterizing the compressibility of a liquid. Particularly, it represents how easy a unit volume of a fluid can be changed when changing the pressure applying upon it. The bulk modulus of elasticity is affected by many factors, e.g., pressure, temperature, and undissolved air volume. In the pressurization process, the liquid pressure changes over time, leading to a change of the bulk modulus. The relationship between the chamber pressure and bulk modulus of Mil-PRF-83282 is shown in Fig. 2.

According to the pressure requirement, since the pressure in the chamber is in the range of 0–100 bar, so the relationship between the chamber pressure and the bulk modulus can be considered as linear (Fig. 2). The relationship can be described by the following equation:

$$B = c P_{\text{chamber}} + d. \tag{6}$$

The pressure in the pump chamber is designed to be less than 100 bar, so it is possible to approximate the relationship between bulk modulus and liquid pressure as a linear relationship with a value of $c = 0.1$ and $d = 1.7e4$. Moreover, the pump chamber has O-ring seals to prevent leakage. Since the

O-ring seal is made of rubber, the O-ring is compressed as the chamber pressure increases. That changes the volume of the chamber. Suppose the relationship between the chamber pressure and the volume change caused by the compressed O-ring is expressed as Eq. (7):

$$V_0 = g(P_{\text{chamber}}). \tag{7}$$

Then, substituting (7), (6), and (5) into (2) leads to the motion of the piston equally under the compressibility and the chamber pressure:

$$\frac{x A_{\text{piston}} - g(P_{\text{chamber}})}{V_{\text{chamber}}} = \frac{P_{\text{chamber}}}{c P_{\text{chamber}} + d}$$

$$\therefore \; x = \frac{1}{A_{\text{piston}}} \left(\frac{P_{\text{chamber}} V_{\text{chamber}}}{c P_{\text{chamber}} + d} + g(P_{\text{chamber}}) \right). \tag{8}$$

Substituting (8) into (5) results in the relationship among the chamber pressure and the piston dimension as well as the changed chamber's volume due to deformation of the O-ring:

$$k \frac{1}{A_{\text{piston}}} \left(\frac{P_{\text{chamber}} V_{\text{chamber}}}{c P_{\text{chamber}} + d} + g(P_{\text{chamber}}) \right)$$
$$= F_{\text{a}} - P_{\text{chamber}} A_{\text{piston}}. \tag{9}$$

In this study, the ball-type check valve was used, with the area ratio of 1. Thus, the pressure in the load side will increase gradually until it is equal to the maximum chamber pressure. Therefore, the determination of the maximum chamber pressure is useful for evaluating the saturated pressure value in the load side. The pressurization process can be described in the flowchart shown below (Fig. 3).

It can be seen that the pressure in the load side is always less than or equal to the chamber pressure. Thus, the maximum chamber pressure is the saturation value of the pressure in the load side. To determine the pressure value in the chamber, the relationship between the pressure and deformation
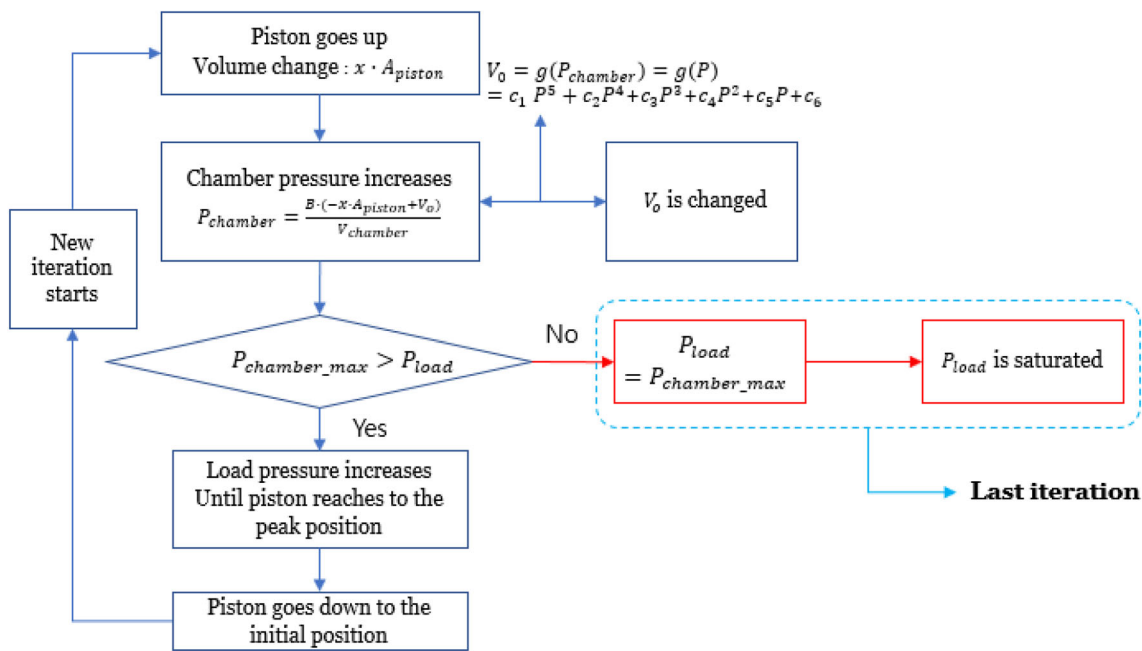
Fig. 3 The pressurization process flowchart

of the O-ring should be determined ($V_0 = g(P_{\text{chamber}})$). This is discussed in the next section.

4 Effect of an O-ring Seal on the Pressurization Process

Because of their adaptability and simple manufacturability, O-rings are presently the most broadly used type of seals in the industry. O-rings are used in both static and dynamic applications and perform an important role in the shipping, industrial machinery, building machinery, as well as in household appliances. Static seals are applied between two stationary surfaces. Dynamic seals are used between surfaces, which are either reciprocating or rotating relative to each other. In this study, there are two positions using O-ring seals. One is the dynamic seal which is around the piston (Fig. 4) and the other is the static seal which is around the chamber (Fig. 5). Both seals have the same C/S (cross-sectional diameter) of 2 mm. The ID (inner diameter) of the seal surrounding the chamber is 36 mm. For the O-ring installed around the piston, the inner diameter is between 20 and 30 mm, depending on the diameter of the piston.

With the O-ring installed around the piston, its movement is associated with the movement of the actuator. Deformation of the O-ring caused by the two causes which are the fluid pressure and the friction with the pump body during the movement. The piston displacement is very small compared to the size of the O-ring, so the friction created during the motion can be ignored. The change in fluid pressure was con-

sidered the reason for the O-ring deformation in this study. Figures 4a and 5a show the O-ring before installation. The O-rings fit in the housing with overlap, which creates initial preload after assembly, Figs. 4 and 5b. This preload and the liquid pressure apply to O-ring together to form the sealing effect. The O-ring is pushed to the side of the groove and when O-ring deforms, the pressure is assigned to the surrounding surfaces (Figs. 4, 5c). The variation of the chamber's volume which caused by seal compression due to the acting pressure can be estimated by the calculation of the volume change of space around the seals.

4.1 Constitutive Modeling of the O-ring

Compared to relatively rigid metal, rubber is a hyperelastic material. Its parameters are commonly defined by the constitutive model. In subsequent simulation calculations, the constitutive model of hyperelastic materials, e.g., the Neo-Hookean model, the Mooney–Rivlin model, and the Yeoh model, can be directly used in this simulation. Because the Mooney–Rivlin model is generally used and its accuracy recognized by many studies, the Mooney–Rivlin model was used for defining the parameters in this paper.

The constitutive model is widely showed in the strain energy density equations used for hyperelastic materials. In this work, the strain energy density equations of the Mooney–Rivlin model of rubber material are as follows:

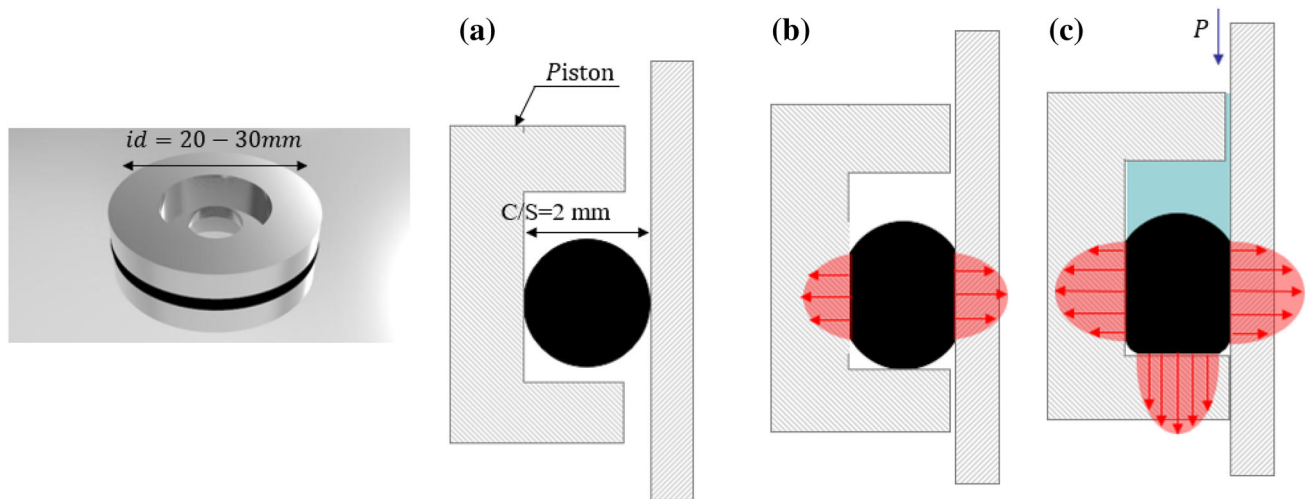$$W = C_{10}(I_1 - 3) + C_{01}(I_2 - 3), \tag{10}$$

Fig. 4 Operating principle of O-ring around the piston. **a** Before installation, **b** preload after installation, and **c** under liquid pressure
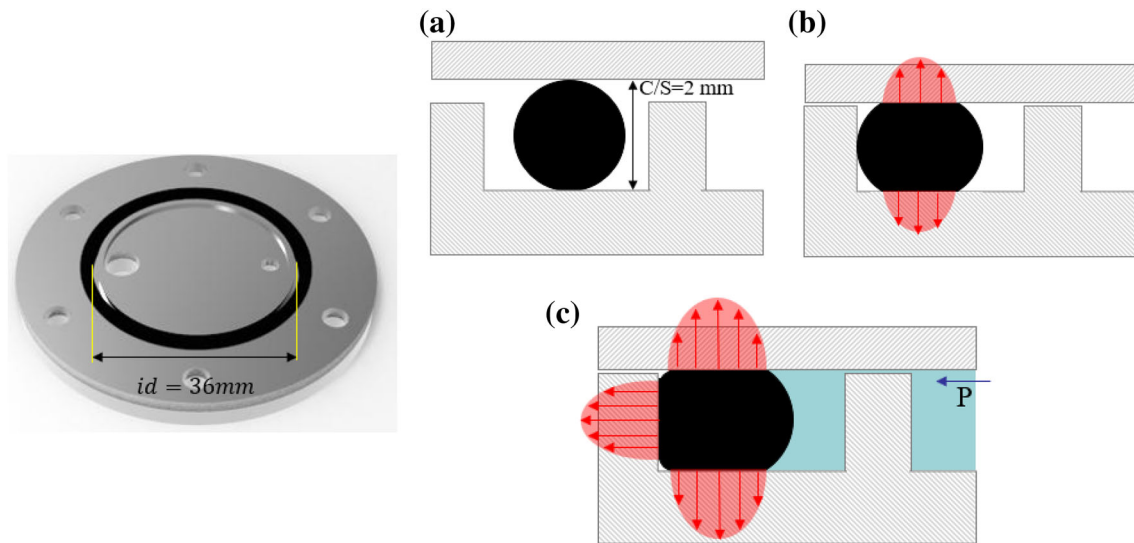

Fig. 5 Operating principle of O-ring around the chamber. **a** Before installation, **b** preload after installation, and **c** under liquid pressure

where I_1 and I_2 are two strain invariants, while C_{10} and C_{01} are two Mooney constants achieved by stress–strain fitting. The relationship of stress and strain can be achieved by the following:

$$\frac{\sigma_1}{2\left(\lambda_1^2 - \frac{1}{\lambda_1}\right)} = C_{10} + \frac{1}{\lambda_1}C_{01}, \tag{11}$$

where σ_1 and λ_1 are the amount of stress and the percentage of strain, respectively. Both parameters are achieved by mechanical experiments. The stress–strain data are used in Eq. (10) to get the values for the material parameters of rubber, $C_{10} = 0.2$ MPa, and $C_{01} = 6$ MPa. These parameters can be identified in the data sheet of the material properties provided by manufactures.

4.2 Finite-Element Model of the O-ring

For the O-ring finite-element simulation, an axisymmetric model was applied. This model contains three parts, namely the O-ring, the piston, and the pump body. In the simulation, only the O-ring will be compressed, so very small reduced parts of the piston and pump body are modeled in the simulation. The reduced geometry helped to decrease the number of elements which used in the FE model and to save the computational simulation time. The nominal dimensions of the parts can be seen in Figs. 6 and 7. First, an FE simulation that is based on the nominal dimensions was conducted. Second, the chamber pressure considering effect of O-ring deformation was taken into account.
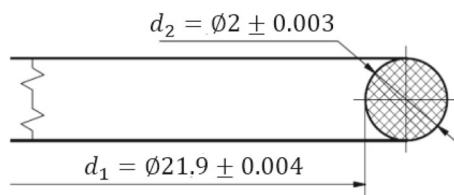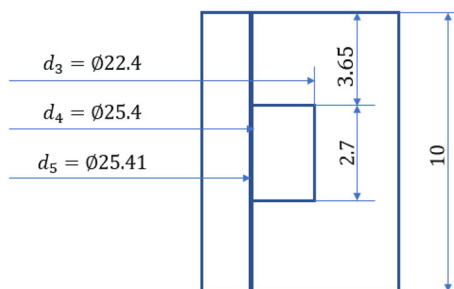
Fig. 6 The dimensions of the O-ring

Fig. 7 The dimension of the piston and the pump body

Fig. 8 FE mesh of the O-ring and the contacting parts

The O-ring was chosen to have a 22.4 mm inside diameter and a 2 mm cross-sectional diameter, which are commonly used dimensions. The dimensions of the housing were designed in case the static pre-stress of the O-ring is about 25% with nominal dimensions. Figure 8 illustrates the mesh of the FE model, where triangular and quadratic rectangular elements were used. The element size is 0.025 mm on the O-ring, 0.1 mm on the pump body, and 0.1 mm on the piston with local refinements. 0.01 mm elements were used on the edges of the O-ring, so that the fluid pressure can go through gradually into the O-ring and the contacting components. During the simulations, fixed constraints were applied to the piston and on the pump body. Only the O-ring was able to deform. The coefficient of friction between the contacting components and the O-ring was defined as 0.2. The contact option used for the connections between the parts was the Augmented Lagrange with aggressive, automatic normal contact stiffness update. The maximum pressure of the O-ring was from 0 to 80 bar with a sinusoidal form that applied downwards vertically on the O-ring. The simulations were carried out in ANSYS Workbench 18.0 software.

Figure 9 shows the time curve of the FE simulation. First, the O-ring is installed into its groove with overlap. ANSYS program automatically softens the normal contact stiffness between the contacting parts and the O-ring. As a result, the ANSYS software eliminates the overlap and the O-ring deforms into the space by the time of 0.004 s. The liquid pressure is gradually applied on the upper semicircle of the O-ring by the end of 0.00816 s in order to display the time-dependent behavior.
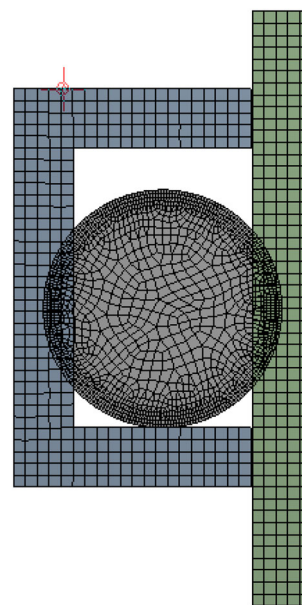
4.3 FEA Results of the O-ring

4.3.1 Results for Nominal Case

In terms of displacement, the maximal displacement at $t = 0.004$ s occurs to be at the side of the O-ring which at it contacts the contacting parts, as shown in Fig. 10. This is due to the initial compression of the O-ring. After applying the liquid pressure, the maximal displacement happens at the upper right and left corners of the O-ring. This is because the O-ring fills out the space and touches the space's lower side. After applying load, the O-ring is significantly different from the original shape. Furthermore, the friction force prevents the O-ring from recovering its original shape. Because of the large displacement and the existence of friction, high strain values are seen in this area. Large displacement values can also be noticed at the side of the O-ring which is connected to the pump body (Fig. 10b). This shows that the contact pressure is greater in this region. Figure 11 expresses the equivalent true strain of the O-ring. It can be seen that the maximal equivalent at both sides is different due to the effect of the tolerance. This is because the existence of friction between the O-ring and the piston or the pump body tries to prevent the O-ring to enter into the gap. Because of the friction and the constantly applied pressure, the material lengthens along the contacting parts, so high strain and stress happen. Because the contact area of the O-ring seal against the pump body is small, it leads to a small friction force compared with the force generated by the actuator. Therefore, the friction force between the O-ring seal and the pump body was ignored in the simulation.

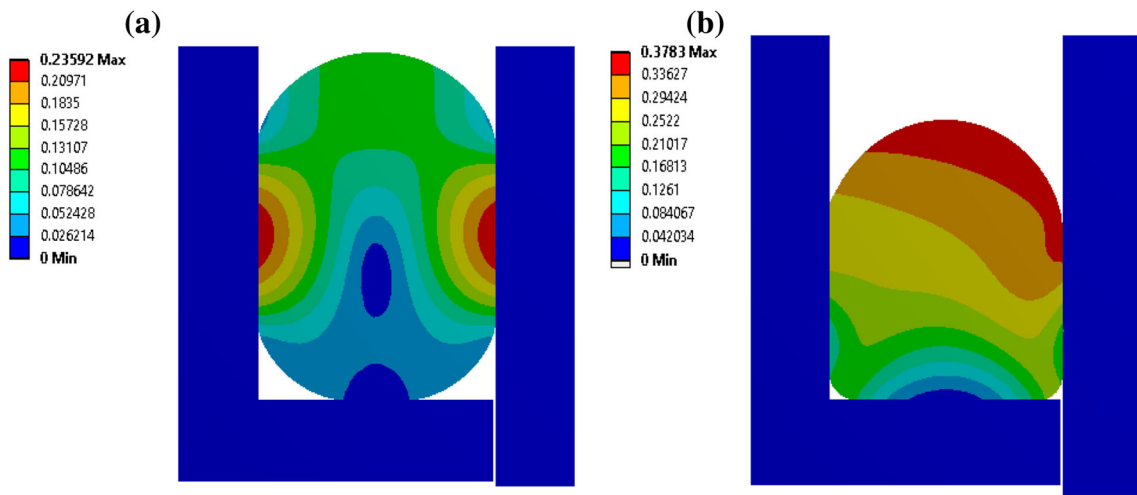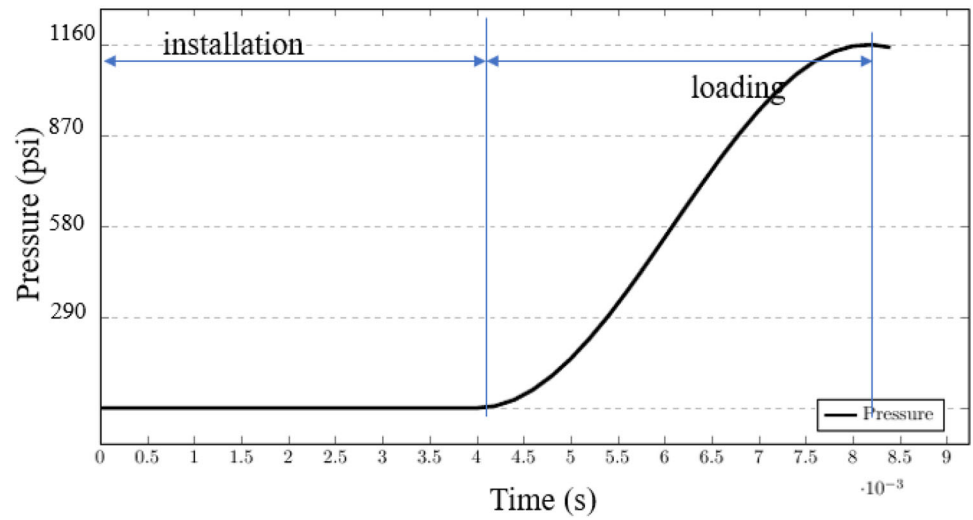**Fig. 9** The time of the installation and the pressure build-up process

Fig. 10 Total displacement of the O-ring. **a** Initial compression; **b** loading (maximum 50 bar)
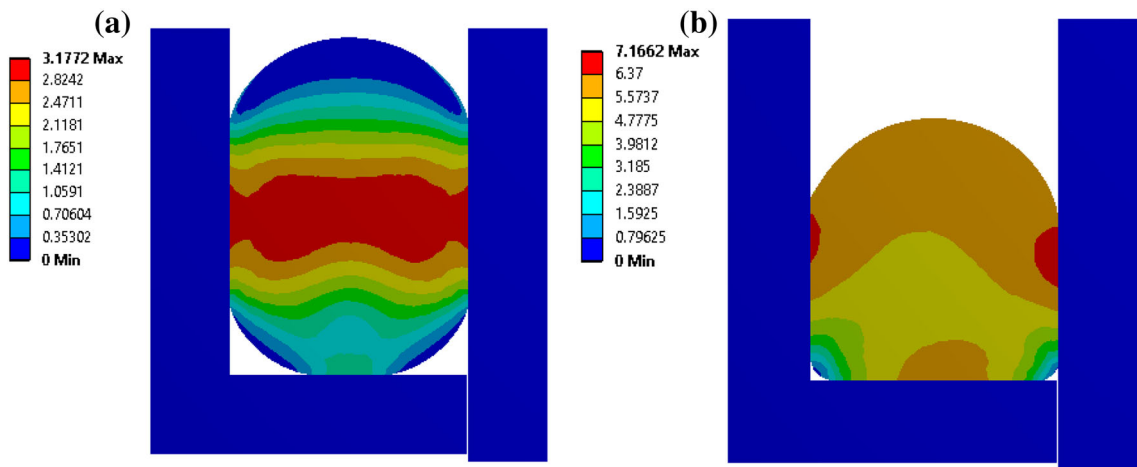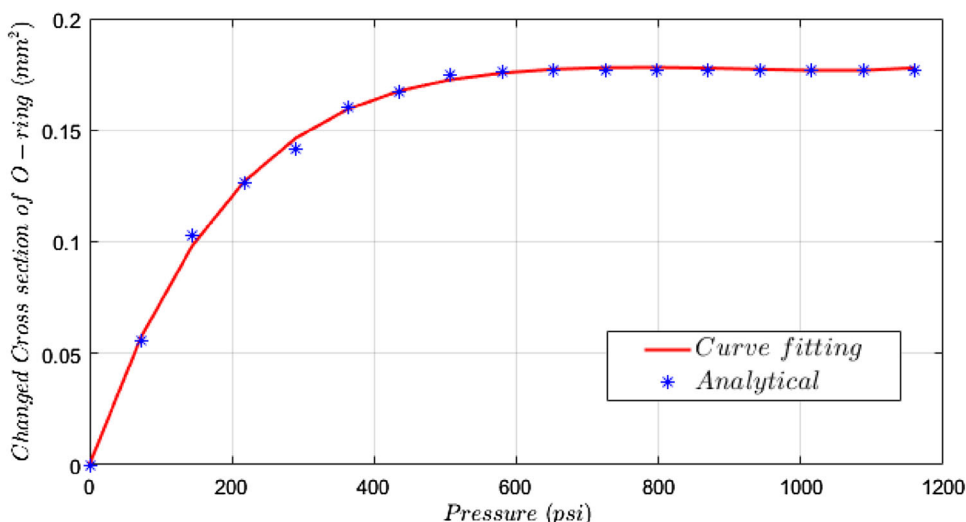

Fig. 11 Equivalent true strain of the O-ring. **a** Initial compression; **b** loading

4.3.2 Effect of the Chamber Pressure on the Chamber Volume

In the pressurization process, the volume change of the chamber caused by the O-ring deformation is the volume. Figure 12 shows the chamber volume change during loading (red line) compared with the initial stage. In the loading stage, the chamber pressure increases and the O-ring is compressed which leads to the volume of the chamber expanding until the O-ring is no longer deformable. For the O-ring used in this study, until the chamber pressure value reaches about 600 psi, the O-ring is not deformed anymore. Therefore, the chamber volume is unchanged when the chamber pressure value increases. In fact, the friction between the O-ring and the surrounding parts prevents it from returning into its original shape. That leads to a change in chamber volume compared to the volume at the initial compression stage. Thus, the difference in these two results (the chamber volume change in the loading stage and the initial stage), as shown in Fig. 12, is the volumetric variation of the chamber during the liquid pressure increase. It can be seen that the volume change of the O-ring, in this case, is unchanged when the chamber pressure exceed 600 psi.

In other words, the difference between the two main processes is the chamber volume change during the pressurization caused by the O-ring seal compression process. The relationship of the chamber pressure and the changed chamber volume is shown in Fig. 12.

The relationship shown in Fig. 12 will be approximated by an algebraic function that can be used as $g(P_{chamber})$ in Eq. (8). The approximated function has the form as shown in the following:

$$V_0 = g(P_{chamber}) = g(P)$$
$$= c_1 P^5 + c_2 P^4 + c_3 P^3 + c_4 P^2 + c_5 P + c_6. \quad (12)$$

Fig. 13 Components of the designed piezoelectric-hydraulic pump

By determining the relationship between the change in chamber volume and the chamber pressure, the maximum pressure in the chamber will be determined according to Eq. (10). The results are discussed in the next section.

5 Experimental Verification for the Saturated Load Pressure

5.1 Performance Test of the Manufactured Piezoelectric-Hydraulic Pump Brake System

An actual piezoelectric-hydraulic pump, shown in Fig. 13, was manufactured to validate the performance of the designed piezoelectric-hydraulic pump for the UAV brake system. The different parts of the designed piezoelectric-hydraulic pump were modularized to easily facilitate part replacement.

Fig. 14 The load pressure corresponds to piston diameter value $d = 30$ mm
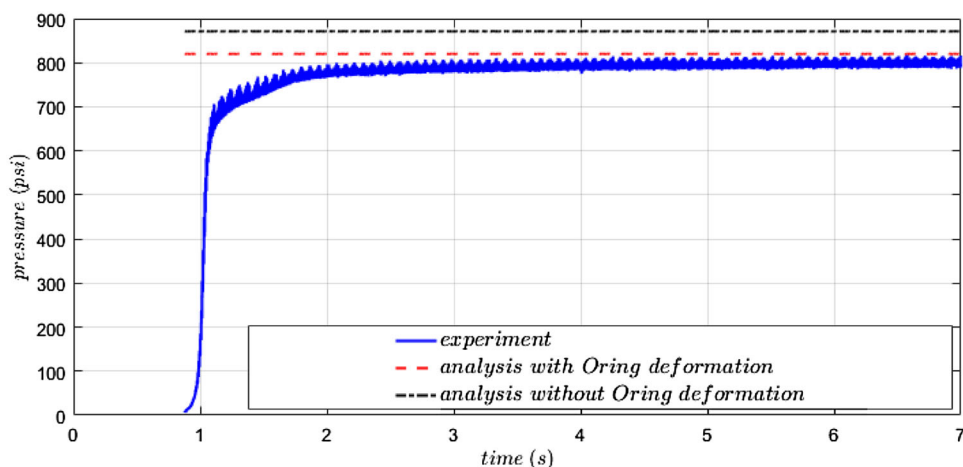
These elements were created by precision machining and the check valves were manufactured using wire-cut electric discharge machining, because they have a complicated shape and thin plate. The produced parts of the piezoelectric-hydraulic pump brake system are illustrated in Fig. 13.

For the performance test of the designed piezoelectric-hydraulic pump used in UAV brake system, the experimental devices such as a DAQ program, a high-voltage amplifier, a pressure sensor, a solenoid valve, and an electronic scale were constructed, as shown in Fig. 1. The high-voltage amplifier amplifies the generated signal and applies it to the piezoelectric actuator at a given driving frequency. The DAQ program 'dSPACE' enables the collection and creation of the digital and analog signal data. The high-voltage amplifier, E-481 model by PI Company, was used to supply the high-voltage output at the driving frequency of 120 Hz.

The solenoid valve connected to the exhaust port of the piezoelectric-hydraulic pump played an important role in the exhaust performance test of the pump. If the solenoid valve was opened, the flow rate in the no-load state could be measured. When the solenoid valve was closed, a closed-loop hydraulic circuit such as that in a brake system formed. The pressure of the load side was measured using a pressure sensor. Concerning the medium, Mil-PRF-83282, widely used in actual aircraft hydraulic brake systems, was used in this study.

The experiments on the pressurization process for the designed piezoelectric-hydraulic pump brake system were carried out according to the following process. Firstly, the On/Off solenoid valve connected to the exhaust port was closed. Once the solenoid valve was closed, the flow path from the check valve of the exhaust port of the piezoelectric-hydraulic pump to the solenoid valve formed a closed-loop hydraulic circuit such as that in a brake system. Next, the input voltage was subsequently applied to the stacked piezoelectric actuator while changing the driving frequency. Finally, the load pressure of the piezoelectric-hydraulic

pump brake system was measured using the pressure sensor.

5.2 Experimental Results and Discussion

In the following, we analyzed the maximum pressure in the chamber with some voltage applied to the actuator. As can be seen in Fig. 14, the simulation predicting the load side pressure indicates good agreement with those results obtained from the experimental data. The load side pressure will increase over time until the saturation value is reached. This value is equal to the maximum pressure in the chamber, because the area ratio of the check valve is 1.

The maximum pressure value at the load side is equal to the maximum pressure in the chamber when the check valve with a value area ratio of 1 is used. With no regard for deformation of the O-ring ($g(P_{chamber}) = g(P) = 0$), the chamber pressure is greater about 12%. Therefore, when analyzing the pump which has a small chamber, the influence of O-ring should be considered. Besides, it is important to note the time taken to obtain the required load side pressure of the brake system. Increasing the pressure at the load side until reaching the maximum value depends on the liquid volume at the load side. For the brake system, it is necessary to require the pressure value to reach the required value in a short period of time. Therefore, in the design phase, the volume at the load side requires attention in terms of the required time. Equation (9) allows us to directly predict the performance of a piezoelectric-hydraulic pump. It is well known that many factors exert influence on the pressurization performance of the pump, such as driving voltage, chamber height, O-ring seal properties, the radius of the piston, valve type/size, and liquid properties. Besides determining the maximum pressure value in the chamber, this work also estimates the effect of the piston's radius on the maximum pressure value. To verify the analytical result, a piezoelectric-hydraulic pump brake system (presented Fig. 15) was fabricated and tested

Fig. 15 Pistons with different diameters were used in the experiment

20mm   24mm   25.4mm   27mm   30mm
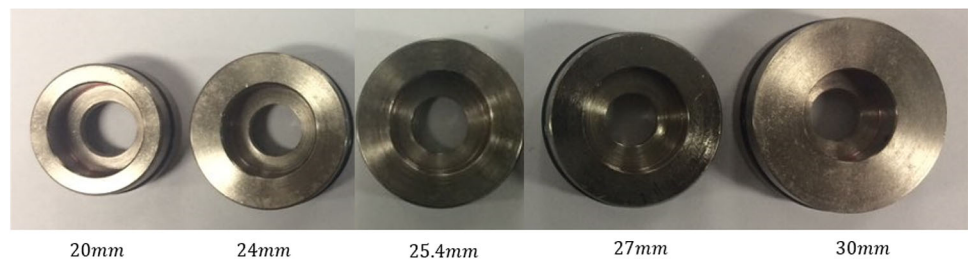
for the maximum pressure value at 900 V. To obtain the influence of the piston's radius on the maximum pressure value, five different sizes of pistons (Ø20/24/25.4/27/30 mm) were utilized for experiments.

To highlight the effect of the piston's radius on the performance of the piezoelectric-hydraulic pump brake system, the pressurization process was tested with the same driving voltage.

From the curves in Fig. 16, we can find that the optimal piston diameter for the piezoelectric-hydraulic pumps brake system to achieve the maximal pressure is about 25.5 mm. This suggests that the radius of piston affects the maximum chamber pressure significantly. In the case of disregard for deformation of the O-ring, the optimum value of the piston diameter is about 24.9, and the pressure in the cavity is much larger than the value of the test. According to the presented results, the maximum load side pressure of the pump can also be enhanced by decreasing the changed volume of the O-ring due to the pressure. In the analytical results which showed in Figs. 14 and 16, there were slight differences in values compared to the experimental results of the actual hydraulic pump. This occurred, because the fluid–structure interaction (FSI) dynamic behavior of the check valve and the check valve shape which affect on the opening of the check valve was not considered in the analytical method. Therefore, for more accurate results, the FSI dynamic behavior and the check valve shape had to be included to perfectly obtain the relationship between the load side pressure and the chamber pressure. In addition, in the case of the actual piezoelectric-hydraulic pump used in the brake system, fluctuations in the pressure occurred due to the imperfect sealing of the check valve. However, it was impossible for the check valves to perfectly synchronize with the piezoelectric actuator without leakage from the intake and exhaust unit. That leads to a difference between the analytical results and experimental results, although it is not so great. Therefore, it is concluded that the analytical result for load side pressure was calculated properly.

6 Conclusions

In this paper, the effect of an O-ring deformation on the chamber pressure of the small piezoelectric-hydraulic pump brake system has been investigated. Due to the O-ring seal made

of rubber, the nonlinear behavior of the O-ring should be taken into account. The FEM simulation has been used to analyze the volume change of any O-ring size with increasing pressure. The analytical results showed that the O-ring seal is compressed and then the chamber volume increases as the chamber pressure increases. However, when the chamber pressure is increased to a certain value, the O-ring cannot be deformed anymore. Then, the volume of the chamber is not influenced by O-ring deformation. The chamber volume at this time depends only on the displacement of the piston, which is proportional to the pressure in the chamber. For the O-ring used in this study, this pressure value is about 600 psi. Besides, when the pressure is removed, the O-ring cannot return to its original shape due to the influence of friction. Although the deformation of the O-ring is not large, its effect is very significant when it is used for the small piezoelectric-hydraulic pump.

The simulation results predicting saturated pressure show a good match with those obtained from the experiment. In terms of liquid compressibility, the chamber pressure rises with the increasing of the piston radius and the piston displacement. On the other hand, the increasing the piston radius will result in an increased transmission surface, which reduces the pressure in the chamber. Thus, there will be an optimal piston radius for the piezoelectric-hydraulic
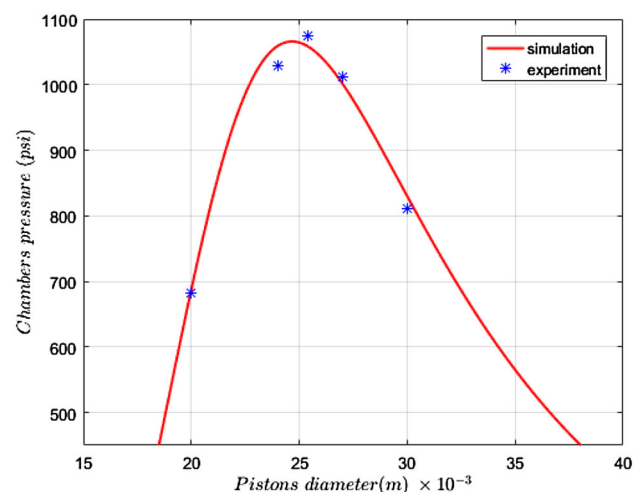

Fig. 16 Influence of the piston diameter on the maximum pressure value

pump to achieve the maximum chamber pressure, i.e., the maximum pressure in the load side. With the O-ring used in this study, the optimum piston diameter value is about 25.4 mm with the maximum saturated pressure of 1030 psi. The obtained results also show that the decreasing O-ring seal deformation leads to increasing saturated pressure in the load side. Consequently, the pressurization performance of the piezoelectric-hydraulic pump brake system has been enhanced.

References

1. Ma HK, Hou BR, Wu HY, Lin CY, Gao JJ, Kou MC (2008) Development and application of a diaphragm micro-pump with piezoelectric device. J Microsyst Technol 14(7):1001–1007

2. Cazorla PH et al (2014) Piezoelectric micro-pump with PZT thin film for low consumption microfluidic devices. J Procedia Eng 87:488–491

3. Larson JP, Dapino MJ (2012) Reliable, high-frequency miniature valves for smart material electrohydraulic actuators. J Intell Mater Syst Struct 23(7):805–813

4. Laser DJ, Santiago JG (2004) A review of micropumps. J Micromech Microeng 14(6):35–64

5. Iverson BD, Garimella SV (2008) Recent advances in microscale pumping technologies: a review and evaluation. J Microfluid Nanofluid 5(2):145–174

6. Chaudhuri A, Wereley N (2012) Compact hybrid electrohydraulic actuators using smart materials: a review. J Intell Mater Syst Struct 23(6):597–634

7. Ullmann A (1998) The piezoelectric valve-less pump—performance enhancement analysis. J Sens Actuators Phys 69(1):97–105

8. Kim HH, Oh JH, Lim JN, Lim KJ, Park DH (2009) Design of valveless type piezoelectric pump for micro-fluid devices. J Procedia Chem 1(1):353–356

9. Zhang JH, Wang Y, Huang J (2017) Advances in valveless piezoelectric pump with cone-shaped tubes. J Mech Eng 30(4):766–781

10. Kan JW, Yang ZG, Peng TJ, Cheng GM, Wu B (2005) Design and test of a high-performance piezoelectric micropump for drug delivery. J Sens Actuators Phys 121(1):156–161

11. Fan ZQ, Liu J, Dong JS, Li JQ, Jiang B (2009) Study on the large flow rate piezoelectric mini-pump with metal check valve. In: International conference on mechatronics and automation, pp 4294–4298

12. Ren YJ, Ma YT, Huang D, Chen J, Feng JH (2016) Elastic string check valves can efficiently heighten the piezoelectric pump's working frequency. J Sens Actuators Phys 244:126–132

13. Lin QM, Yang B, Xie J, Tai YC (2006) Dynamic simulation of a peristaltic micropump considering coupled fluid flow and structural motion. J Micromech Microeng 17(2):220–228

14. Jang LS, Kan WH (2007) Peristaltic piezoelectric micropump system for biomedical applications. J Biomed Microdevices 9(4):619–626

15. Liang L, Ma X, Zhang T (2012) Structure design and simulation of circular ring piezoelectric peristaltic pump. J Chin Soc Agric Eng 28:40–44

16. Li B, Chen Q, Lee DG, Woolman J, Carman GP (2005) Development of large flow rate, robust, passive micro check valves for compact piezoelectrically actuated pumps. J Sens Actuators Phys 117:325–330

17. Choi SB, Yoo JK, Lee YS (2005) Position control of a cylinder system using a piezoactuator-driven pump. J Mechatron 15(2):239–249

18. Hwang JH, Bae JS, Hwang YH, Kwon JY (2018) Pressurization characteristics of a piezoelectric-hydraulic pump for UAV brake systems. Int J Aeronaut Space Sci 19(3):776–784

19. Hwang JH, Bae JS, Yang J, Kwon JY (2014) The design on the spring sheet type check valve of smart material hydraulic pump. In: The society for aerospace system engineering, Fall Conference Paper #85

20. Hwang LJ, Yang J, Joo Y, Bae JS, Kwon JY (2015) Design of the compound smart material pump for brake system of small and medium size UAV. J Soc Aerosp Syst Eng 9(3):1–7

21. Lee HJ, Hwang JH, Bae JS, Kwon JY (2014) Conceptual design of compound smart material pump with sequential operation of fluid displacement–force. In: The society for aerospace system engineering, Spring Conference Paper #95

22. Lindler JE, Anderson EH, Regelbrugge ME (2003) Design and testing of piezoelectric-hydraulic actuators. In: Proceedings of the 9th SPIE conference on smart structures and integrated systems, San Diego, CA Paper #5054-11